Materials Research Express

PAPER

# The influence of temperature on preparing tungsten doped vanadium dioxide films by sol-gel method

To cite this article: Shuliang Dou *et al* 2019 *Mater. Res. Express* **6** 016408



Materials Research Express

PAPER

# The influence of temperature on preparing tungsten doped vanadium dioxide films by sol-gel method

RECEIVED
19 July 2018

REVISED
14 September 2018

ACCEPTED FOR PUBLICATION
24 September 2018

PUBLISHED
10 October 2018

**Shuliang Dou**[1,3], **Weiyan Zhang**[2,3], **Yuemin Wang**[1], **Yi Wang**[1], **Xiang Zhang**[1], **Leipang Zhang**[1], **Lebin Wang**[1], **Jiupeng Zhao**[2,4] and **Yao Li**[1,4]

[1] Centre for Composite Material and Structure, Harbin Institute of Technology, Harbin, People's Republic of China
[2] School of Chemical Engineering and Technology , Harbin Institute of Technology, 150001, Harbin, People's Republic of China
[3] These authors contributed equally to this work.
[4] Authors to whom any correspondence should be addressed.

**E-mail:** yaoli@hit.edu.cn **and** jpzhao@hit.edu.cn

**Keywords:** vanadium dioxide, sol-gel method, optics, thermochromic film, smart window

Supplementary material for this article is available online

## Abstract

The influence of annealing temperature on the preparation of W- doped $VO_2$ films is investigated in the paper. W dopant is introduced by pouring the melt $V_2O_5$ into ammonium tungstate solution. And the W- doped $VO_2$ films are obtained via dip-coating method followed by annealing at argon atmosphere. The evolution of crystal structure, valence value of surface element, surface morphology, roughness and thermochromic performance are studied at different temperature. And different concerntration of W doped $VO_2$ (M) films are prepared by the same method, which exhibit excellent performance. The proposed technique provides a path for fabricating W- doped $VO_2$(M) solar modulating coatings.

## 1. Introduction

Vanadium dioxide is a widespread interesting material since its novel metal-insulator transition (MIT), accompanied with distinct optical tunability in selective near-infrared [1]. It changes from metal state with opaque in near infrared regions to insulator with transparency at 68 °C [2]. The unique property has a promising application on smart device, such as microbolometers or field effect transistor [3], storage systems [4], sensors [5], electronic switching devices [6], and smart windows [7–9].

However, vanadium dioxide thin films have not been used in practical applications owing to their slightly higher transition temperature ($T_t$) compared to room-temperature (RT). Doping is an effective way to reduce the $T_t$. Particularly, the $T_t$ is shifted to RT by doping films with high-valence ions, for instance, molybdenum [10] and tungsten [11]; as well as silicon [12] and fluorine [13]. Among these dopants, tungsten is found to be most effective, lowering $T_t$ by 23 °C per 1 at% [14–16]; while 15 °C per 1 at% has also been reported for Mo [17].

However, the perfect stoichiometric $VO_2$ is difficult to fabricate because of the abundant vanadium oxides, such as $V_3O_5$, $V_2O_5$, [18] and so on. Besides, the main phases of $VO_2$ exist four forms, $VO_2$(A), $VO_2$(B) and $VO_2$(M/R), which have stable structures in similar conditions during $VO_2$ growth [19]. Even so, a wide range of methods are applied for $VO_2$ (M)-based film fabrication, such as sol-gel [20], magnetron sputtering deposition [21], wet chemical approaches [22, 23], chemical vapor deposition (CVD) [24], thermolysis method [25], and pulsed laser deposition (PLD) [26]. The sol-gel method is a low cost, facile coating on large scale surface, easy control of reaction kinetics and atomic doping and lower sintering temperature way to prepare $VO_2$ film [20, 27, 28]. In a typical sol-gel process for $VO_2$ synthesis, costly tetravalent alkoxide precursor, such as vanadium tetrabutoxide, was coated onto substrates, and then underwent high temperature annealing under inert atmosphere [25]. Up to now, researchers have developed the sol-gel methods for $VO_2$ thin film synthesis. For example, Gao *et al* developed an interesting $VOCl_2$ precursor containing PVP polymer [7, 8, 29–32]. Besides, inorganic sol-gel method is a facile method because its simple process and costless starting material [17, 33, 34].

Huang *et al* reported a involved mixing water with molten $V_2O_5$ powders to obtain $V_2O_5{\cdot}nH_2O$ gels [35]. And the $Mo^{5+}$ and $W^{5+}$ ions were doped into $VO_2$ films by mixing ammonium molybdate and ammonium tungstate with $V_2O_5$ powder following by melting at 800 °C, respectively.

Here, a facile method to prepare W-doped $VO_2$ films has been presented by modifying inorganic sol-gel method. And the W dopant was introduced by pouring the melt $V_2O_5$ into ammonium tungstate solution. And the influence of temperature is investigated in the annealing process from precursor to W-doped films. It seems that the W-doped $VO_2$ (M) film can be obtained at 600 °C, which exhibits excellent performance on smart window. The results support an insight on the understanding of the preparation for W-doped $VO_2$ (M) film by inorganic sol-gel method.

## 2. Experiment

### 2.1. starting material

Vanadium pentoxide powder($V_2O_5$, AR) and Polyvinylpyrrolidone(PVP, K30, AR) were used as starting material to prepare sol, which were purchased from Tianjin Guangfu Fine Chemical Research Institute. Ammonium tungstate (AR) was used as W source. All the reagents were purchased and used without further purification, except for the ammonium tungstate was heated in vacuum oven at 200 °C to remove the adsorbed water.

### 2.2. Preparation of the precursor sol

W-doped precursor sol was fabricated by a water quenching method: 2.5 g $V_2O_5$ powder was melted at 850 °C for 10 min, and then poured into 100 ml ammonium tungstate solution(0.7 g $L^{-1}$) at room temperature (RT). The obtained slurry was stirred vigorously for 1 h, and diluted with de-ionized water(DI-18MΩ) water to 10 g $L^{-1}$. PVP (K30 6 wt%) was introduced to the sol to stabilize the sol at RT. The W-doped precursor sol was obtained after vigorous stirring for 10 h. the amount of doped W element was adjusted by the different concentration of ammonium tungstate solution. And the pure precursor was obtained by the same process, except for pouring melt $V_2O_5$ into DI water. All the samples used in this work were synthesized using these precursor sols, unless otherwise noted.

### 2.3. Fabrication of W-doped $VO_2$ films

Precursor films were deposited on fused-silica substrates (1 × 4 $cm^2$) by dip coating method. After drying for 30 min at 80 °C to remove the excess solvent, the smooth precursor films were formed. These precursor films were then annealed under an argon atmosphere (purity of 99.999%), which was accompanied by crystallization and reduction from the $V_2O_5$ phase to the $VO_2$ phase. And the annealing temperature varied from 400 °C to 650 °C with an interval of 50 °C, and the corresponding samples were signed as WV400, WV450, WV500, WV550, WV600 and WV650. The annealing time was chose as 5 h to ensure complete crystallization. The general fabrication process is illustrated in Scheme 1.

### 2.4. Measurements

The crystalline phases of the films were determined using an x-ray diffraction (XRD) diffractometer (PANalytical B V, Model Xpert Pro, primary monochromatic Cu-Kα radiation). The morphology and thickness of the films were determined by a field-emission scanning electron microscope(SUPRA 55 SAPPHIRE). The surface roughness was measured by an atomic force microscope (AFM, Dimension Icon, Bruker). x-ray photoelectron spectroscopy (XPS) studies were conducted with a PHI 5700 ESCA System using Al Ka radiation (1486.6 eV).

The transmittance of the W-doped $VO_2$ films was measured using a UV–vis – NIR spectrophotometer (Lambda — 950, Perkin Elmer) equipped with a film heating unit over the wavelength range of 250–2500 nm. Hysteresis loops were measured by collecting the transmittance of films at a fixed wavelength (2000 nm) at an approximate interval of 2.0 °C by using a fiber optic spectrometer (Ocean optics, NIRQuest 256–2.5). The temperature was measured with a thermocouple in contact with the film and was controlled by a temperature-controlling unit. The temperature errors were smaller than 0.5 °C based on repeated measurements.

## 3. Results and discussion

### 3.1. Crystal structure

The phase evolution of the W-doped films was characterized by XRD. Figure 1 shows the XRD patterns for the films. And no phase of W based oxide is observed at patterns of all the samples. It is readily seen from the patterns that the sample WV400 is composed of two phases of $VO_2$ (B) (JCPDS 31–1438) and $V_2O_5$ (JCPDS 52–0794),

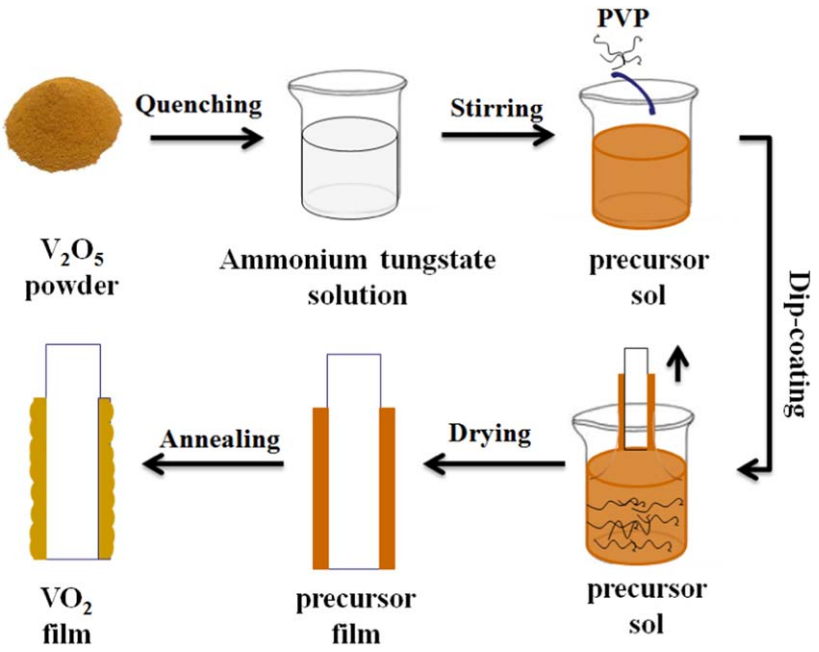


**Scheme 1.** Schematic illustration for the preparation of W-doped $VO_2$ (M) films on both sides of the fused-silica substrates.

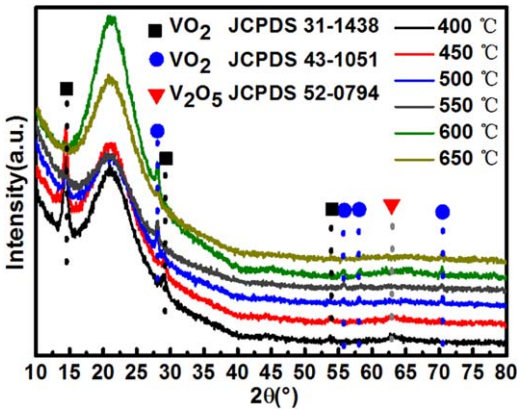


**Figure 1.** XRD patterns of samples prepared at different annealing temperature.

respectively [36–38]. And the main peaks of (011) and (002) crystal planes for B phase $VO_2$ are amplified in the figure S1 is available online at stacks.iop.org/MRX/6/016408/mmedia, which are in 14.4° and 29°, respectively. Besides, the diffraction peaks of the $V_2O_5$ phase is weak and the $VO_2$ (B) is strong, which means the main phase in the sample is $VO_2$ (B). When the annealing temperature increases to 450 °C, the secondary diffraction peak of $VO_2$(B) at 29° is weaker, while the main diffraction peak at 14.4° is still strong (figure S1). No monoclinic phase (JCPDS 43–1051) is observed in pattern of the sample WV450, and a tiny diffraction peak of $V_2O_5$ can be confirmed as $V_2O_5$ at 63.1°. $VO_2$ (M) appears in the pattern of sample WV500 [39–41], acompanying with a relative weak diffraction peak of $VO_2$ (B). And the predominant M phase exhibits a strong diffraction peak at 28°, which can be well assigned to the (011) crystal plane. However, although the intensity of diffraction peak for M phase is enhanced in the pattern of the sample WV550, a slight diffraction peak of $VO_2$(B) still exists at 14.4°. Furthermore, the intensity of diffraction peaks exhibit more stronger for M phase and no other phase is observed at the patterns of the sample WV600. However, as the annealing temperature increasing to 650 °C, the main diffraction peaks of W-doped $VO_2$ film disappears and only a weak peak survives as the (011) plane of M phase. Besides, the broad diffraction peaks at 15°–35° originate from the fused-silica substrates. It seems that higher annealing temperature may degenerate the crystallinity of M phase. Besides, the phase of precursor films change from $V_2O_5$ to $VO_2$ (M) via an intermediate phase of $VO_2$ (B). Furthermore, no coexist of three phases is observed in all the patterns, which is different to the phase transformation of pure $VO_2$ (M) film [42].

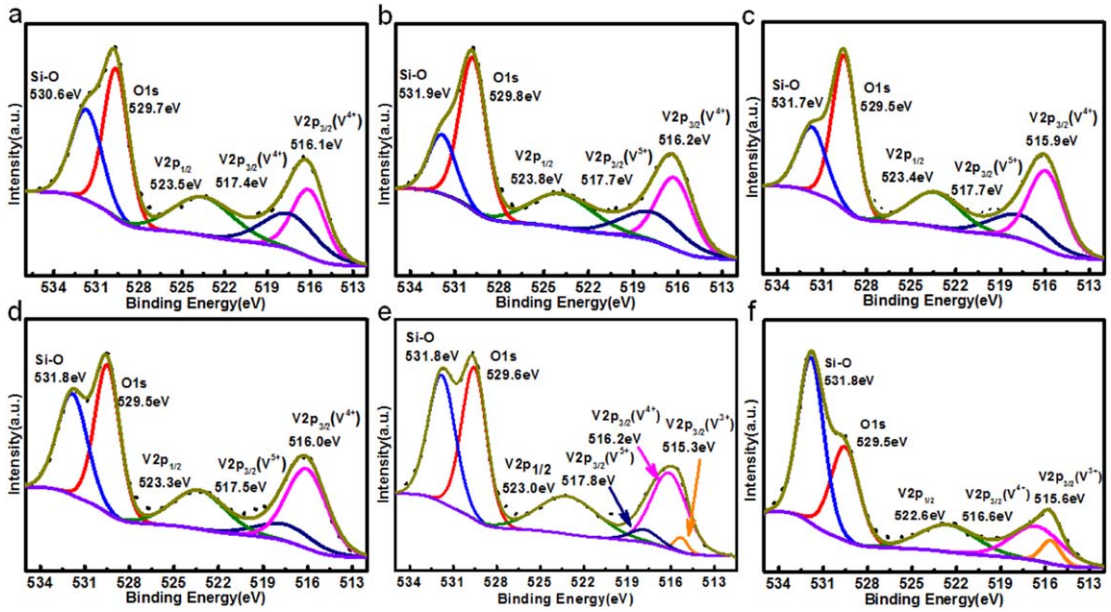


**Figure 2.** High-resolution XPS profiles of $V_{2p}$ and $O_{1s}$ for the films annealed at different temperature: (a)–(f), WV400–WV650.

### 3.2. XPS analysis

The evolution of surface chemical composition and their valence states of the W- doped films annealed at different temperature are investigated by XPS. The valence states of V element are show in figure 2. It seems that the valence states of V element in different samples vary obviously and comprise $V^{5+}$, $V^{4+}$ and $V^{3+}$. For the sample WV400, as shown in figure 2(a), the deconvolution peak of V $2p_{3/2}$ spectrum can be resolved into two components of 517.4 eV and 516.1 eV, which can be attributed to $V^{5+}$ and $V^{4+}$, respectively [43–45]. As the annealing temperature increasing, the V $2p_{3/2}$ spectra of WV450, WV500 and WV550 can be still deconvoluted into $V^{5+}$ and $V^{4+}$, respectively (figure 2(b)), and the intensity of $V^{4+}$ deconvolution peak enhances gradually. Furthermore, the $V^{4+}$/V ratio in the samples enlarged as the temperature increasing (table S1). Three valence states of $V^{5+}$, $V^{4+}$ and $V^{3+}$ coexists in the sample WV600, simultaneously. And it suggests that it difficult to prepare pure M phase W-doped $VO_2$ film. And the $V^{4+}$/V ratio increases to largest of 83.8%(table S1). Furthermore, the $V^{5+}$ valence state of W-doped $VO_2$ film disappears when the annealing temperature increased to 650 °C, accompanying with lower $V^{4+}$/V ratio.

The corresponding deconvolution peak of $W_{4f}$ spectra in the samples are also investigated. As show in figure S2, the W element exists as $W^{6+}$ in all the films [11, 20, 46], which means that the value state of W element have no change throughout all the annealing temperature. Besides, the W/W + V ratio varied randomly, which means the complicated phase transformation process from $V_2O_5$ to $VO_2$.

Since the precursor sol comprises three typical N element of –C-N, W-N and $NH^{4+}$, the evolution of N is traceed at different annealing temperature to understand the annealing process insightfully. As shown in figure S3, it seems that the deconvolution peaks in profiles of the samples degenerated as the annealing temperature increasing. And it is corresponding to the decomposition of PVP and $NH^{4+}$ in the W doped films. Besides, the existence of $N_{1s}$ deconvolution peak suggests that N residual in the sample W650 (figure S3(f)), which means the uncompleted decomposing of PVP.

### 3.3. Surface morphology

The evolution of the surface morphology of the films was investigated by SEM. As shown in figure 3, it suggests that the sample WV400and WV450 are smooth and dense(figures 3(a) and (b)), and the films WV500, WV550, WV600 and WV650 are compose of micro-structure (figures 3(c), (d) and (e)). However, it seems that the sample WV500 is comprised of dense submicro particles. And the smaple WV550 is consist of inhomogeneous component in the surface. Furthermore, the surface of sample WV600 is ice-crystal like microstructure, which is simliar to the undoped $VO_2$ film annealed at 500 °C. Besides, the film WV650 is consist of dense particles on the surface, and the grain diameter is about one hundred nanometer. It seems that the change on the film surface texture with increasing annealed temperature can be stributed to the effects of surface tension and the complex decomposing process of precursor gel film.

The AFM measurement is used to investigated the variation of microstructure in height of the samples, as shown in figure 4. The samples exhibit the same evolutions as the SEM results. Furthermore, the average

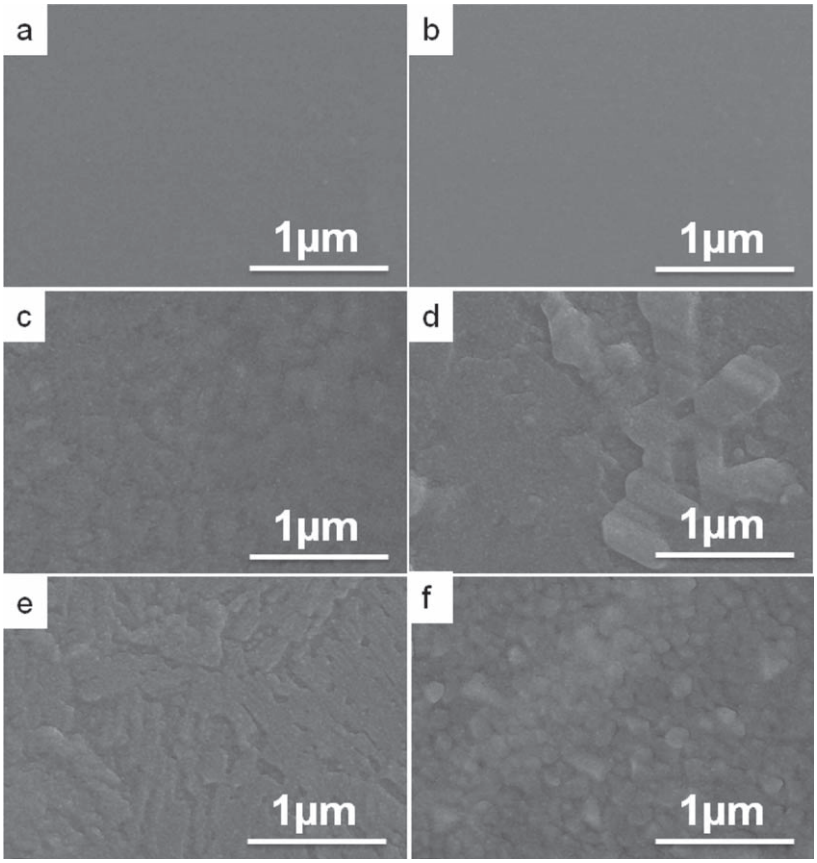


**Figure 3.** The surface microstructure of W-doped $VO_2$ films annealed at different annealing conditions: (a)–(f), WV400–WV650.

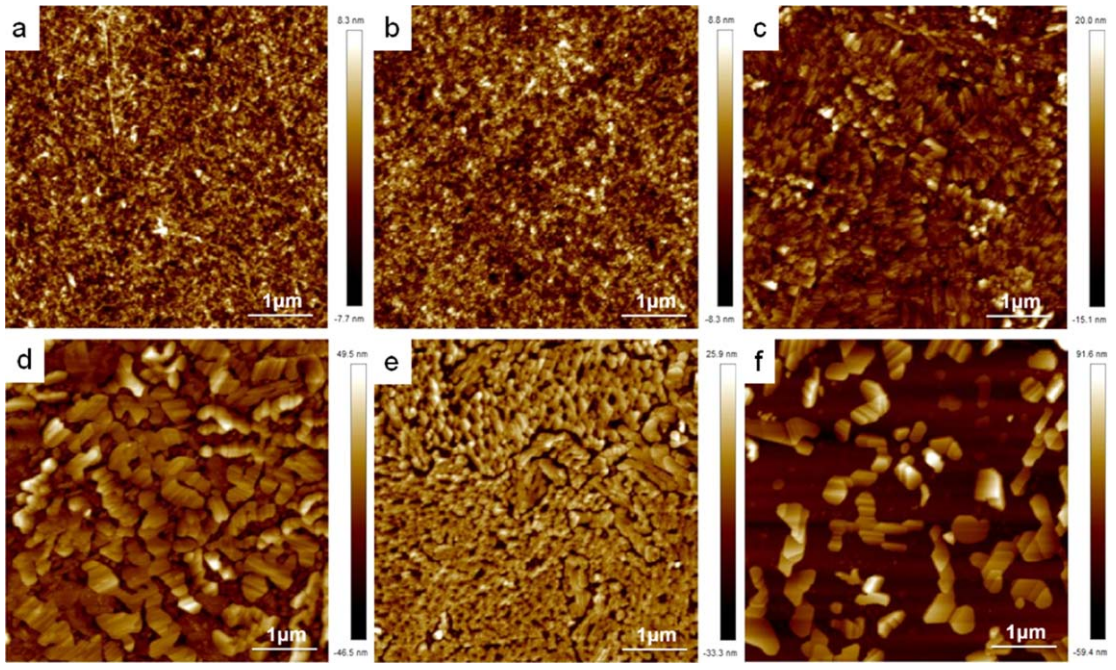


**Figure 4.** AFM images of $VO_2$ (M) films: (a)–(f), WV400–WV650.

roughness values ($R_a$, $R_q$) and maxium roughness values ($R_{max}$) of the samples are shown in figure S4(a). The roughness of the samples increases with the annealing temperature, which means the distinct morphology changes in the annealing process. And the $R_a$ and $R_q$ changes from several nanomenters (WV400) to the finally resulting of dozen nanometers in height (WV650). Besides, the $R_{max}$ is overwhelmed the $R_a$ and $R_q$, which means

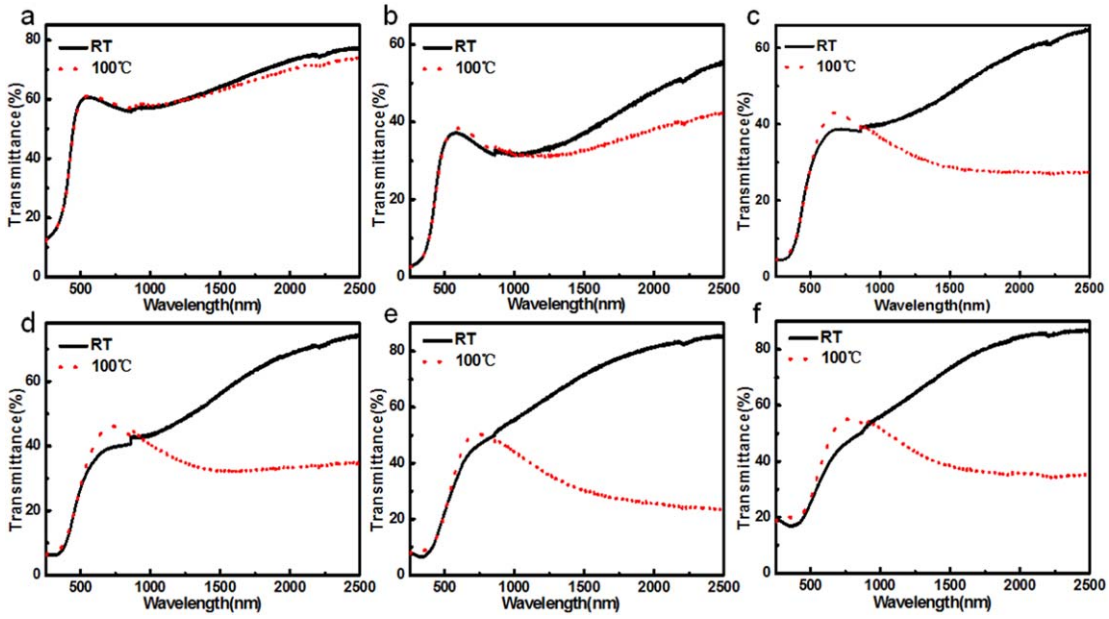


**Figure 5.** The transmittance and reflectance spectra of the samples annealed at different temperature: (a)–(f), WV400–WV650. The corresponding reflectance spectra collected at RT. The solid and dashed lines are collected at RT and 100 °C, respectively.

the uneven surface of the samples. Interestingly, the roughness of sample WV600 lower those value of both WV550 and WV650. It can be seen from the AFM images that the WV600 is composed of more smaller micro-structure, which lead to lower roughness.

### 3.4. Thermochromic performances

The transmittance spectra of the W-doped films annealed at different temperature are investigated at RT and 100 °C, which corresponds to the two states of the $VO_2$ (M) film. As shown in figure 5, the variation of transmittance for different samples is significant difference at near infrared wavelength. The variation of transmittance at 2000 nm between RT and 100 °C is defined as $\Delta T_{2000nm}$, which is obtained by equation (1):

$$\Delta T_{2000nm} = T_{2000nm}(M) - T_{2000nm}(R) \quad (1)$$

Where the $T_{2000nm}(M/R)$ is the $_{transmittance}$ at 2000 nm measured at RT and 100 °C, respectively.

The $\Delta T_{2000nm}$ of the samples is gradually enlarged as the annealing temperature increasing to 600 °C and slightly lowered at 650 °C (figure. S3(b)). And it seems that the $\Delta T_{2000nm}$ changes with the component of $VO_2$(M) phase in the films. The $\Delta T_{2000nm}$ of samples W1and W2 is very small, which is attributed to the rarely $VO_2$ (M) phase in the films. And the samples W3 and W4 shows larger $\Delta T_{2000nm}$, where the $VO_2$(M) is main phase in the films. Furthermore, the WV600 exhibits the largest $\Delta T_{2000nm}$ in all the samples, which is in accordance with the dominated $VO_2$(M) phase and the largest $V^{4+}/V$ ratio in the film. Besides, the $\Delta T_{2000nm}$ of sample WV650 degenerates slightly but still larger than those of WV400, WV450, WV500 and WV550. It seems that the 'particle' surface of sample W6 enhance the transmittance at 100 °C, which lead to smaller $\Delta T_{2000nm}$ compared with W5.

Typically, the main optical performances of $VO_2$ thermochromic smart windows, including luminous transmittance ($T_{lum}$, 390–780 nm) and solar modulate ability ($\Delta T_{sol,}$ 250–2500 nm), are obtained using the following equations:

$$T_{1um/sol} = \int \varphi_{1um/sol}(\lambda) T(\lambda) d\lambda \Big/ \int \varphi_{1um/sol}(\lambda) d\lambda \quad (2)$$

$$\Delta T_{sol} = T_{sol}(30\ ^\circ C) - T_{sol}(100\ ^\circ C) \quad (3)$$

where $T(\lambda)$ is the recorded film transmittance, $\varphi_{lum}$ is the standard luminous efficiency function for the photopic vision of human eyes, and $\varphi_{sol}$ is the solar irradiance spectrum for air mass 1.5 (corresponding to the Sun at 37° above the horizon).

The $T_{lum}$ and $\Delta T_{sol}$ of the samples are calculated by equations (2) and (3). As shown in figure S3(b), the $\Delta T_{sol}$ shows the same evolution as the $\Delta T_{2000nm}$ in different samples, while the $T_{lum}$ is opposite. And the $T_{lum}$ changes slightly in the samples W4, W5 and W6. Especially, the sample WV600 exhibits overwhelming $\Delta T_{sol}$ and the smallest $T_{lum}$ compared to others, which may be the result of the coupling interaction between crystal structure and surface morphology.

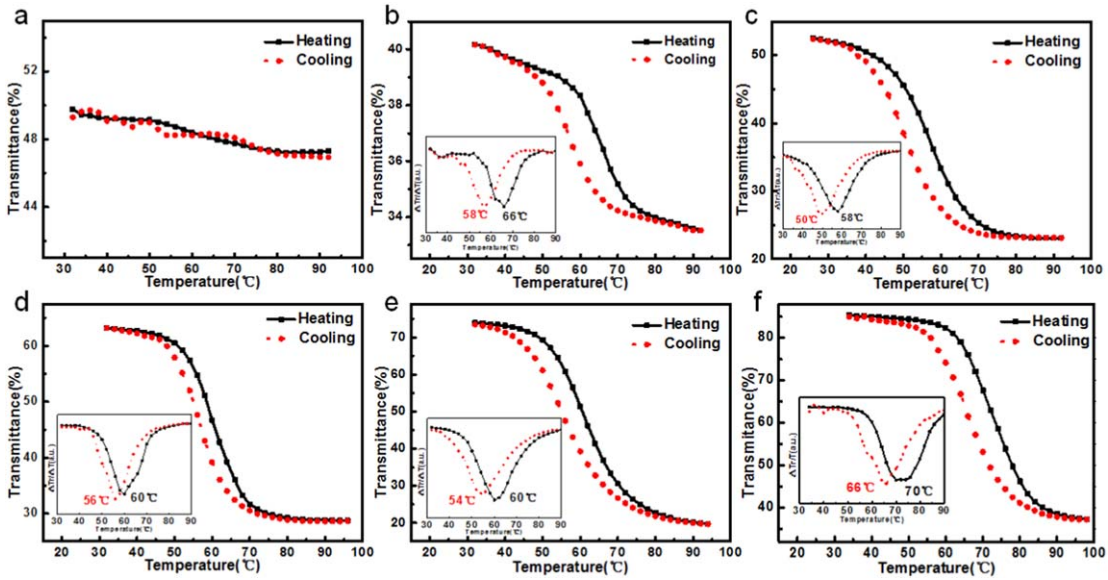


**Figure 6.** The hysteresis loops of the samples annealed at different temperature: (a)–(f), WV400–WV650. The insets are the corresponding $d(T_r)/d(T)$–T curves. The solid and dashed lines are collected in heating and cooling processes, respectively.

**Table 1.** The phase transition temperature and hysteresis loops width of the samples.

| Samples | $T_h$ | $T_c$ | $T_t$ | $\Delta T$ |
|---|---|---|---|---|
| W400 | — | — | — | — |
| W450 | 66 | 58 | 62 | 8 |
| W500 | 58 | 50 | 54 | 8 |
| W550 | 60 | 54 | 57 | 6 |
| W600 | 60 | 54 | 57 | 6 |
| W650 | 70 | 64 | 67 | 6 |

The hysteresis loops of the films were measured by recording the transmittance variation in heating and cooling processes at 2000 nm, as shown in figure 6. It can be seen that the Sample WV400 exhibits no hysteresis loops. And the other samples show obvious hysteresis loops, which means the existing $VO_2$(M) in the films.

The $d(T_r)/d(T)$–T curves were used to describe the definition of the transition parameters of heating and cooling branches. The temperature corresponding to the peak is defined as the phase transition temperature of the heating and cooling branches, denoted as $T_h$ and $T_c$, respectively. For cooling branches with the appearance of two peaks in the $d(T_r)/d(T)$ –T curves, the $T_c$ values are determined by the main peak. The phase transition temperature ($T_t$) of the film is defined as average value of $T_h$ and $T_c$. The hysteresis loop width ($\Delta T_t$) is defined as the difference between $T_h$ and $T_c$. The phase composition, the optical performances, transition temperature and hysteresis loop width of the films are summarized in table 1. The $T_t$ of all the samples is lower than the pure $VO_2$ film of 68 °C. And the $\Delta T$ is more narrow than that of pure $VO_2$ film. And the sample WV600 shows $T_t$ of 57 °C and $\Delta T$ of 6 °C.

## 4. Conclusions

In conclusion, the influence of annealing temperature on preparation of W-doped $VO_2$ films by inorgance sol method is investigated. The phase changes from $V_2O_5$ to $VO_2$(M) via an intermediate phase of $VO_2$(B) without coexistance of three phases. Besides, the valence of V element exists three velence state in the W-doped $VO_2$(M) films. Furthermore, the N element in the PVP develops to the N residual on the $VO_2$ surface. And the surface roughness of the samples enlarges as the annealed temperature increasing, except for a slight reduce at 600 °C. The ratio of W and V element changes at the annealing process, which suggest the complex formation of W-doped $VO_2$ film. Besides, the optimized annealing temperature is 600 °C accompanied with largest $\Delta T_{sol}$ and pure M phase $VO_2$. And the phase transition temperature is lowered by the introduced W dopant. The proposed technique gives an insight understanding for preparing W-doped $VO_2$(M) solar modulating coatings.

## Acknowledgments

We thank National Natural Science Foundation of China (No.51572058, 51502057), National Key Research & Development Program (2016YFB0303903, 2016YFE0201600), the International Science & Technology Cooperation Program of China (2013DFR10630, 2015DFE52770), and Foundation of Equipment Development Department (6220914010901).

## ORCID iDs

Yao Li https://orcid.org/0000-0003-3859-8135

## References

[1] Morin F J 1959 Oxides which show a metal-to-insulator transition at the neel temperature *Phys. Rev. Lett.* **3** 34–6
[2] Beteille F and Livage J 1998 Optical switching in $VO_2$ Thin Films *J. Sol-Gel Sci. Technol* **13** 915–21
[3] Chen C and Zhou Z 2007 Optical phonons assisted infrared absorption in $VO_2$ based bolometer *Appl. Phys. Lett.* **91** 011107
[4] Roach W R 1971 Holographic storage in $VO_2$ *Appl. Phys. Lett.* **19** 453–5
[5] Liu H, Rua A, Vasquez O, Vikhnin V S, Fernandez F E, Fonseca L F, Resto O and Weisz S Z 2005 Optical and nonlinear optical response of light sensor thin films *Sensors* **5** 14
[6] Yang Z, Ko C and Ramanathan S 2011 Oxide electronics utilizing ultrafast metal-insulator transitions *Annual Review of Materials Research* **41** 337–67
[7] Kang L, Gao Y and Luo H 2009 A novel solution process for the synthesis of $VO_2$ thin films with excellent thermochromic properties *ACS Appl. Mater. Interfaces* **1** 2211–8
[8] Chen Z, Gao Y F, Kang L T, Du J, Zhang Z T, Luo H J, Miao H Y and Tan G Q 2011 $VO_2$-based double-layered films for smart windows: optical design, all-solution preparation and improved properties *Sol. Energy Mater. Sol. Cells* **95** 2677–84
[9] Li R, Ji S D, Li Y M, Gao Y F, Luo H J and Jin P 2013 Synthesis and characterization of plate-like $VO_2$(M)@$SiO_2$ nanoparticles and their application to smart window *Mater. Lett.* **110** 241–4
[10] Jiazhen Y, Yue Z, Wanxia H and Mingjin T 2008 Effect of Mo-W Co-doping on semiconductor-metal phase transition temperature of vanadium dioxide film *Thin Solid Films* **516** 8554–8
[11] Liang Z, Zhao L, Meng W, Zhong C, Wei S, Dong B, Xu Z, Wan L and Wang S 2017 Tungsten-doped vanadium dioxide thin films as smart windows with self-cleaning and energy-saving functions *J. Alloys Compd.* **694** 124–31
[12] Gao Y Z, Xu Y Q, Cao Y and Hu C W 2012 Introducing organosilicone source into the synthetic system of polyoxovanadates: two novel {V15Si6O48}-based extended chains *Dalton T* **41** 567–71
[13] Dai L, Chen S, Liu J J, Gao Y F, Zhou J D, Chen Z, Cao C X, Luo H J and Kanehira M 2013 F-doped $VO_2$ nanoparticles for thermochromic energy-saving foils with modified color and enhanced solar-heat shielding ability *Phys. Chem. Chem. Phys.* **15** 11723–9
[14] Hu L, Tao H, Chen G, Pan R, Wan M, Xiong D and Zhao X 2015 Porous W-doped $VO_2$ films with simultaneously enhanced visible transparency and thermochromic properties *J. Sol-Gel Sci. Technol.* **77** 85–93
[15] Zhang Y, Zhang X, Huang Y, Huang C, Niu F, Meng C and Tan X 2014 One-step hydrothermal conversion of $VO_2$(B) into W-doped $VO_2$(M) and its phase transition and optical switching properties *Solid State Commun.* **180** 24–7
[16] He X, Zeng Y, Xu X, Gu C, Chen F, Wu B, Wang C, Xing H, Chen X and Chu J 2015 Orbital change manipulation metal-insulator transition temperature in W-doped $VO_2$ *Phys. Chem. Chem. Phys.* **17** 11638–46
[17] Mai L Q, Hu B, Hu T, Chen W and Gu E D 2006 Electrical property of Mo-Doped $VO_2$ nanowire array film by melting-quenching sol-gel method *J. Phys. Chem.* B **110** 4
[18] Bahlawane N and Lenoble D 2014 Vanadium oxide compounds:structure, properties, and growth from the gas phase *Chem. Vapor Depos.* **20** 299–311
[19] Strelcov E, Tselev A, Ivanov I, Budai J D, Zhang J, Tischler J Z, Kravchenko I, Kalinin S V and Kolmakov A 2012 Doping-based stabilization of the M2 phase in free-standing VO(2) nanostructures at room temperature *Nano Lett.* **12** 6198–205
[20] Pan G, Yin J, Ji K, Li X, Cheng X, Jin H and Liu J 2017 Synthesis and thermochromic property studies on W doped $VO_2$ films fabricated by sol-gel method *Sci. Rep.* **7** 6132
[21] Zhang D-P, Zhu M-D, Liu Y, Yang K, Liang G-X, Zheng Z-H, Cai X-M and Fan P 2016 High performance $VO_2$ thin films growth by DC magnetron sputtering at low temperature for smart energy efficient window application *J. Alloys Compd.* **659** 198–202
[22] Gao Y F, Wang S B, Luo H J, Dai L, Cao C X, Liu Y L, Chen Z and Kanehira M 2012 Enhanced chemical stability of $VO_2$ nanoparticles by the formation of $SiO_2$/$VO_2$ core/shell structures and the application to transparent and flexible $VO_2$-based composite foils with excellent thermochromic properties for solar heat control (vol 5, pg 6104, 2012)*Energy & Environmental Science* **5** 9947–9947
[23] Gao Y, Wang S, Kang L, Chen Z, Du J, Liu X, Luo H and Kanehira M 2012 $VO_2$–Sb:$SnO_2$ composite thermochromic smart glass foil *Energy & Environmental Science* **5** 8234–7
[24] Chang H L M, Gao Y, Guo J, Foster C M, You H, Zhang T J and Lam D J 1991 Heteroepitaxial growth of $Tio_2$, $VO_2$, and $Tio_2$/$Vo_2$ multilayers by mocvd *J Phys Iv* **1** 953–60
[25] Wang N, Magdassi S, Mandler D and Long Y 2013 Simple sol–gel process and one-step annealing of vanadium dioxide thin films: synthesis and thermochromic properties *Thin Solid Films* **534** 594–8
[26] Ranjbar M, Mahdavi S M and Iraji zad A 2008 Pulsed laser deposition of W–V–O composite films: preparation, characterization and gasochromic studies *Sol. Energy Mater. Sol. Cells* **92** 878–83
[27] Seyfouri M M and Binions R 2017 Sol-gel approaches to thermochromic vanadium dioxide coating for smart glazing application *Sol. Energy Mater. Sol. Cells* **159** 52–65
[28] Jinhua L, Chan H L W, Chenglu L and Ningyi Y 2004 Comparison of VO 2 thin films prepared by inorganic sol-gel and IBED methods *Applied Physics A: Materials Science & Processing* **78** 777–80
[29] Kang L, Gao Y, Zhang Z, Du J, Cao C, Chen Z and Luo H 2010 Effects of annealing parameters on optical properties of thermochromic $VO_2$ films prepared in aqueous solution *J. Phys. Chem.* C **114** 1901–11

[30] Du J, Gao Y, Luo H, Kang L, Zhang Z, Chen Z and Cao C 2011 Significant changes in phase-transition hysteresis for Ti-doped $VO_2$ films prepared by polymer-assisted deposition *Sol. Energy Mater. Sol. Cells* **95** 469–75
[31] Kang L, Gao Y, Luo H, Chen Z, Du J and Zhang Z 2011 Nanoporous thermochromic VO(2) films with low optical constants, enhanced luminous transmittance and thermochromic properties *ACS Appl. Mater. Interfaces* **3** 135–8
[32] Du J, Gao Y, Chen Z, Kang L, Zhang Z and Luo H 2013 Enhancing thermochromic performance of $VO_2$ films via increased microroughness by phase separation *Sol. Energy Mater. Sol. Cells* **110** 1–7
[33] Liu D, Cheng H, Xing X, Zhang C and Zheng W 2016 Thermochromic properties of W-doped $VO_2$ thin films deposited by aqueous sol-gel method for adaptive infrared stealth application *Infrared Phys. Technol.* **77** 339–43
[34] Dou S L, Wang Y, Zhang X, Tian Y L, Hou X M, Wang J, Li X G, Zhao J P and Li Y 2017 Facile preparation of double-sided $VO_2$ (M) films with micro-structure and enhanced thermochromic performances *Sol. Energy Mater. Sol. Cells* **160** 164–73
[35] Shi Q, Huang W, Zhang Y, Yan J, Zhang Y, Mao M, Zhang Y and Tu M 2011 Giant phase transition properties at terahertz range in VO(2) films deposited by sol-gel method *ACS Appl. Mater. Interfaces* **3** 3523–7
[36] Guo B B, Wan D Y, Ahmad I, Hongjie L J and Gao Y F 2017 Direct synthesis of high-performance thermal sensitive $VO_2$(B) thin film by chemical vapor deposition for using in uncooled infrared detectors *J. Alloys Compd.* **715** 129–36
[37] Ding Z H, Cui Y Y, Wan D Y, Luo H J and Gao Y F 2017 High-performance thermal sensitive $VO_2$(B) thin films prepared by sputtering with TiO2(A) buffer layer and first-principles calculations study *RSC Adv.* **7** 29496–504
[38] Srivastava A *et al* 2015 Selective growth of single phase $VO_2$(A, B, and M) polymorph thin films *APL Materials* **3** 026101
[39] Zhou M, Bao J, Tao M, Zhu R, Lin Y, Zhang X and Xie Y 2013 Periodic porous thermochromic $VO_2$(M) films with enhanced visible transmittance *Chem Commun (Camb)* **49** 6021–3
[40] Chen Z, Cao C X, Chen S, Luo H J and Gao Y F 2014 Crystallised mesoporous $TiO_2$(A)-$VO_2$(M/R) nanocomposite films with self-cleaning and excellent thermochromic properties *Journal of Materials Chemistry* A **2** 11874–84
[41] Dong B R, Shen N, Cao C X, Chen Z, Luo H J and Gao Y F 2016 An abnormal phase transition behavior in $VO_2$ nanoparticles induced by an M1-M2-R process: two anomalous high (> 68 degrees C) transition temperatures *RSC Adv.* **6** 50521–8
[42] Dou S, Wang Y, Zhang X, Tian Y, Hou X, Wang J, Li X, Zhao J and Li Y 2017 Facile preparation of double-sided $VO_2$ (M) films with micro-structure and enhanced thermochromic performances *Sol. Energy Mater. Sol. Cells* **160** 164–73
[43] Silversmit G, Depla D, Poelman H, Marin G B and De Gryse R 2004 Determination of the V2p XPS binding energies for different vanadium oxidation states (V5+ to V0+) *J. Electron Spectrosc. Relat. Phenom.* **135** 167–75
[44] Mendialdua J, Casanova R and Barbaux Y 1995 XPS studies of V205, V6013, $VO_2$ and V203 *J. Electron Spectrosc. Relat. Phenom.* **71** 12
[45] Zhang J *et al* 2016 Thermochromic $VO_2$ films from ammonium citrato-oxovanadate(iv) with excellent optical and phase transition properties *J. Mater. Chem.* C **4** 5281–8
[46] Shen N, Dong B, Cao C, Chen Z, Liu J, Luo H and Gao Y 2016 Lowered phase transition temperature and excellent solar heat shielding properties of well-crystallized $VO_2$ by W doping *Phys. Chem. Chem. Phys.* **18** 28010–7